Home | Browse | Search | My Settings | Alerts | Help

Quick Search   All fields [   ]   Author [   ]
search tips   Journal/book title [   ]   Volume [   ] Issue [   ] Page [   ]   Clear ✗   Go →   Advanced Search

📄 **PDF (761 K)**   📤 Export Citation   ✉ E-mail Article

Article | Figures/Tables (13) | References (15)   Thumbnails | Full-Size Images

doi:10.1016/j.orgel.2009.12.007 | How to Cite or Link Using DOI

◆ Permissions & Reprints

Cited By in Scopus (0)

Solution processed polymer tandem cell utilizing organic layer coated nano-crystalline TiO$_2$ as interlayer

Won-Suk Chung[a, c], Hyunjung Lee[a], Wonmok Lee[b], ✉, Min Jae Ko[a], Nam-Gyu Park[a], Byeong-Kwon Ju[c] and Kyungkon Kim[a], ✉

[a] Materials Science and Technology Division Solar Cell Research Center, Korea Institute of Science and Technology (KIST), Seoul 136-791, Republic of Korea
[b] Department of Chemistry, Sejong University, 98 Gunja-dong, Gwangjin-gu, Seoul 143-747, Republic of Korea
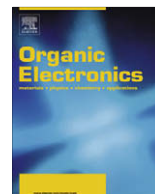
Solution processed polymer tandem cell utilizing organic layer coated nano-crystalline TiO₂ as interlayer

Won-Suk Chung [a,c], Hyunjung Lee [a], Wonmok Lee [b,*], Min Jae Ko [a], Nam-Gyu Park [a], Byeong-Kwon Ju [c], Kyungkon Kim [a,*]

[a] Materials Science and Technology Division Solar Cell Research Center, Korea Institute of Science and Technology (KIST), Seoul 136-791, Republic of Korea
[b] Department of Chemistry, Sejong University, 98 Gunja-dong, Gwangjin-gu, Seoul 143-747, Republic of Korea
[c] Display and Nanosystem Lab, College of Engineering, Korea University, Seoul 136-701, Republic of Korea

ABSTRACT

A solution processed polymer tandem cell has been fabricated by utilizing organic layer coated TiO₂ nanoparticle (OL-TiO₂) as an interlayer. The crystalline phase of the OL-TiO₂ was anatase. The dispersed solution of the OL-TiO₂ showed high optical transparency and excellent film forming property. The top and bottom cell were clearly separated by the OL-TiO₂ interlayer without interlayer mixing, which was not observed for the tandem cell utilizing commercially available TiO₂ nanoparticle (N-TiO₂) as an interlayer. The conversion efficiency of a polymer tandem cell was enhanced from 1.43% to 3.44% by replacing the interlayer from N-TiO₂ to OL-TiO₂. The tandem cell performance was further enhanced by adjusting the thicknesses of the active layers in the subcells and adjusting the conductivity of the PEDOT:PSS layer in the bottom cell. The highest conversion efficiency of 3.66% was obtained from the tandem cell having the structure of ITO/Baytron P VP AI 4083/P3HT:PCBM (100 nm)/OL-TiO₂/Baytron PH 500/P3HT:PCBM (100 nm)/Al. In addition that, it was found that the OL-TiO₂ interlayer enhanced the stability of the tandem cell comparing to that of the single junction cell by the reduction of the oxygen diffusion to the bottom layer by the interlayer. It is expected that the performance of the tandem cell can be further enhanced by adopting efficient low band gap materials.

© 2009 Elsevier B.V. All rights reserved.

1. Introduction

The single junction solar cell has limitations to overcome Shockley–Queisser limitation because excess energy of the photons, absorbed with energies greater than the semiconductor band gap, are lost as heat and photons with energies less than the semiconductor band gap are not absorbed [1]. The tandem solar cell technology could be one way to overcome the limits of the single junction solar cell. However, it is difficult to fabricate polymer tandem solar cells because the previously deposited layer could be destroyed by the following solution process. Therefore, it is important to use a proper separation layer (or interlayer), which isolates two subcells. The interlayer protects the bottom cell as well as recombining the charge carriers from the subcells. There are several reports on the formation of the interlayer and middle electrode by the vacuum deposition method [2–7]. However, it is desirable to fabricate polymer tandem cells with all solution processes in terms of large area fabrication, the production cost and the high throughput. It is essential to develop solution processed interlayer materials to fabricate the polymer solar cell with solution process. Semiconducting metal oxides are thought to be promising candidates for the interlayer due to their optical transparency, electron mobility and chemical stability. Gilot et al., used ZnO nanoparticles/PEDOT interlayer for the
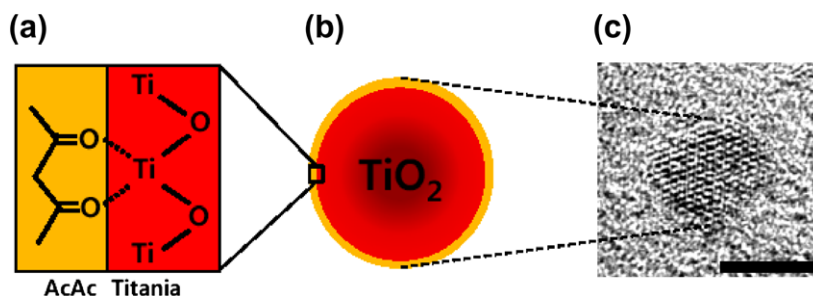
Fig. 1. Organic layer coated TiO_2 nanoparticle used in this study. (a,b) Schematic illustration of the nanoparticle surface where acetylacetone (AcAc) is bound to Ti exposed on the surface (c) HR-TEM image of an individual TiO_2 nanoparticle crystalline lattice. Scale bar represents 5 nm.

polymer tandem cell [8]. However, the neutral pH PEDOT was used for the interlayer instead of commercially available acidic PEDOT:PSS solution due to the chemical instability of the ZnO against the weak acid solution. Recently, Kim et al., successfully fabricated solution processed polymer solar cells by utilizing the TiO_x/PEDOT:PSS interlayer, and the power conversion efficiency reached more than 6% under the 1 sun illumination condition [9]. Thought the TiO_x is promising interlayer material for the polymer tandem cell, the TiO_x layer formation needs a hydrolysis process, which might affect the throughput of the polymer tandem cell production and storage stability of the TiO_x solution is thought to be concerned. The nano-crystalline TiO_2 nanoparticle (NC-TiO_2) is possible candidate material for the interlayer due to their chemical stability, crystallinity and optical transparency. In this study, we fabricated polymer tandem solar cell by using NC-TiO_2 interlayer. Two types of NC-TiO_2 (TiO_2 nanoparticle with or without organic layer on the surface) were utilized as interlayer for the tandem cell. The effects of NC-TiO_2 interlayers on the performance of polymer tandem solar cell will be discussed.

2. Experimental

2.1. Materials and solutions

The P3HT and PCBM blended solution was used to form bulk-heterojunction active layers for the polymer tandem solar cell. The regioregular poly(3-hexylthiophene) (P3HT, Aldrich) and the fullerene derivative [6,6]-phenyl C_{61}-butyric acid methyl ester (PCBM, American Dye Source, Inc.) were dissolved in chlorobenzene with the weight ratio of 1:0.8, and used for active layer of subcells. Three kinds of PEDOT:PSS solutions (Baytron P VP AI 4083, Baytron P, and Baytron PH 500) were purchased from Baytron, H.C. Starck and diluted with methanol by 1:1 vol%. Two types of titanium oxide solution were prepared for the transparent interlayer in the polymer tandem cell. One is the solution that organic layer coated TiO_2 nanoparticles (OL-TiO_2) are dispersed in ethanol. The OL-TiO_2 were synthesized through the hydrolysis of titanium butoxide at 60 °C in the presence of acetylacetone as an organic modifier and p-toluene sulfonic acid as an acid catalyst [10,11]. The mean size and the crystallinity of particles were adjusted by tuning the ratio of reactants. As synthesized

nanoparticles were precipitated in toluene, and redispersed in ethanol by 5 wt% which exhibited a transparent yellow color. The schematic diagram of OL-TiO_2 nanoparticle showing acetylacetone coordinated to TiO_2 at the nanoparticle surface and high resolution transmission electron microscope (HR-TEM) image of an individual nanoparticle are shown in Fig. 1. From the selected area electron diffraction (SAED) on TiO_2 nanoparticles and XRD data, it was confirmed that their crystalline structure of OL-TiO_2 was anatase. The other solution (N-TiO_2) was obtained from the dispersing the TiO_2 nanoparticles (F-6, Showa Denko, Japan) in ethanol by bead-mill. The particle size of the N-TiO_2 was about 15 nm.

2.2. Device fabrication and measurements

The polymer tandem solar cell structure used in this study is shown in the Fig. 2. The tin doped indium oxide (ITO) was used as bottom electrode (BE in Fig. 2) for the tandem cell. The patterned ITO/glass substrates were cleaned in an ultrasonic bath of isopropanol and acetone repeatedly, followed by a UV treatment for 20 min. For the hole injection layer of the bottom cell (HIL in Fig. 2), the PEDOT:PSS aqueous solution (Baytron P VP AI 4083, Baytron P, or Baytron PH 500) was spin-coated onto ITO substrates and dried in the vacuum oven at 120 °C for 10 min. The thickness of the HIL was approximately 40 nm. P3HT:PCBM solution was spun onto the HIL and dried in air at room temperature for 10 min to form a bottom active layer (BL in Fig. 2). Three different thicknesses (70, 100 and 200 nm) of the BL were prepared and the
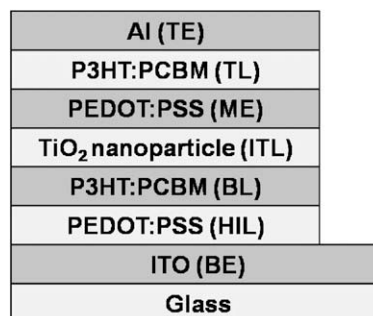

Fig. 2. The polymer tandem cell structure used in this study.

thickness of the layer was controlled by R.P.M of the spin coater. Subsequently, the interlayer (ITL in Fig. 2) for the tandem cell was formed by spinning the TiO_2 nanoparticle solution and drying at 60 °C for 10 min in the vacuum oven. The obtained thickness of the ITL was about 40 nm. Highly conductive PEDOT:PSS (Baytron PH 500, H.C. Starck) was used for the middle electrode (ME in Fig. 2). Since the surface of the ITL is hydrophilic, the aqueous PEDOT:PSS solution can be deposited on it. The same P3HT:PCBM solution was used for the formation of top active layer (TL in Fig. 2). Also, the thickness of the TL was varied from 70 to 200 nm. Finally, Al top electrode (TE in Fig. 2) was vacuum deposited in the base pressure of 2×10^{-6} torr. The thickness of the TE was about 80 nm. The deposited Al electrode area defines an active area of the device as 0.09 cm^2. The prepared tandem cells were directly annealed at 150 °C by a radiation heater for 10 min in the same thermal vacuum evaporator. The base pressure of the evaporator was maintained in the range of 2×10^{-6} to 7×10^{-6} torr.

Photocurrent–voltage measurements were performed on the tandem cells by using a Keithley model 2400 source measuring unit. A class-A solar simulator with a 150 W Xenon lamp (Newport) served as a light source, where its light intensity was adjusted by a NREL-calibrated mono Si solar cell, with a KG-2 filter, for approximately AM 1.5 G 1 sun light intensity. External quantum efficiency was measured as a function of wavelength from 300 to 800 nm using incident photo-to-current conversion system (IPCE) (PV measurements, Inc.). Calibration was performed using a silicon photodiode G425, which was NIST-calibrated as a standard. The atomic force microscopy (AFM) was used to investigate the surface morphology formed by TiO_2 nanoparticle solutions. The AFM measurements were carried out on an Asylum Research MFP-3D-SA AFM mounted on AC160-TS cantilever in noncontact mode. The cross-sectional image of the polymer tandem solar cell was taken with the Dual Beam FIB/SEM system (Nova 200, FEI Company), which allows sectional analysis for the cross-section of delaminated region.

3. Results and discussion

The device structure of the polymer tandem cell used in this experiment is glass/ITO (bottom electrode; BE)/PEDOT:PSS (hole injection layer; HIL)/P3HT:PCBM (bottom active layer; BL)/TiO_2 nanoparticle layer(interlayer; ITL)/PEDOT:PSS (PH 500) (middle electrode; ME)/P3HT:PCBM (top active layer; TL)/Al (top electrode; TE) (Fig. 2). Since this study focuses on the development of the TiO_2 nanoparticle interlayer, the same active layer (P3HT:PCBM) is used for the bottom and top cells.

Two different types of TiO_2 solutions have been examined for the formation of ITL of the polymer tandem cells. The commercially available TiO_2 nanoparticle (F-6, Showa Denko, Japan) was dispersed in ethanol solution (N-TiO_2 solution), and used for the ITL of a polymer tandem cell (TC-N). For the other solution, organic layer (acetylacetone, (AcAc)) coated TiO_2 nanoparticles (OL-TiO_2 solution) were used to form the ITL for another tandem cell (TC-OL). The
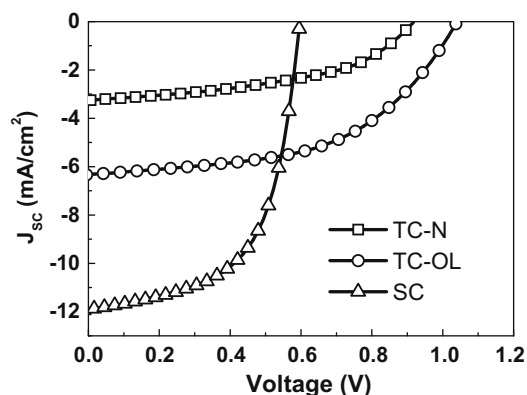

Fig. 3. Current density–voltage characteristics of single junction cell (SC) and tandem cells (TC-N and TC-OL) under the AM 1.5G 1 sun illumination.

N-TiO_2 solution had turbid milky color and precipitated after several days. Whereas, the OL-TiO_2 solution was highly dispersive, transparent and stable over six months without any precipitation.

Fig. 3 shows the current density–voltage characteristics of TC-N and -OL under the AM 1.5 1 sun illumination. The V_{OC} of TC-N (0.92 V) is higher than that of single junction cell (0.6 V). However, there is significant decrease in the J_{SC} and FF of TC-N compared to those of SC. The performance of the tandem cell was enhanced by replacing the interlayer from N-TiO_2 to OL-TiO_2. The V_{OC}, J_{SC} and FF of the tandem cell was increased from 0.92 V, 3.24 mA/cm^2 and 0.48 to 1.04 V, 6.33 mA/cm^2 and 0.52 by changing the interlayer, respectively. As a result, the power conversion efficiency of TC-OL was 3.44% which is 141% higher than that of TC-N (1.43%).

The surface of the interlayer was investigated using atomic force microscopy (AFM). AFM images were obtained after spinning the corresponding TiO_2 nanoparticle solutions on the P3HT:PCBM film. As shown in Fig. 4, large aggregations (ca. 150–300 nm) are observed from the film prepared from the N-TiO_2 solution. The inset of Fig. 4(a) reveals that large aggregations are composed of small nanoparticles (~20 nm). However, no notable aggregation was observed from the surface of the film prepared by the OL-TiO_2 solution (Fig. 4(b)). The RMS roughness of the OL-TiO_2 film was 4.5 nm, which is significantly lower than that of the N-TiO_2 film (87.4 nm). The height profiles of the corresponding film (Fig. 4(c) and (d)) clearly show the difference in the roughness between films. The height of the OL-TiO_2 film is around 10 nm and that of the N-TiO_2 film is in the range of 100–150 nm. However, small voids with size around 30 nm were observed from the OL-TiO_2 film. Those voids are thought to be formed during the solvent evaporation.

The focused ion beam (FIB) image of the TC-OL (Fig. 5(b)) shows the bottom and top cell are clearly separated by the OL-TiO_2/PEDOT:PSS interlayer. In contrast, the TC-N does not show a clear separation of subcells, and large voids (bright region) are observed where the N-TiO_2/PEDOT:PSS ITL is located (Fig. 5(a)). Based on the AFM and FIB experiments, it is believed that the dense
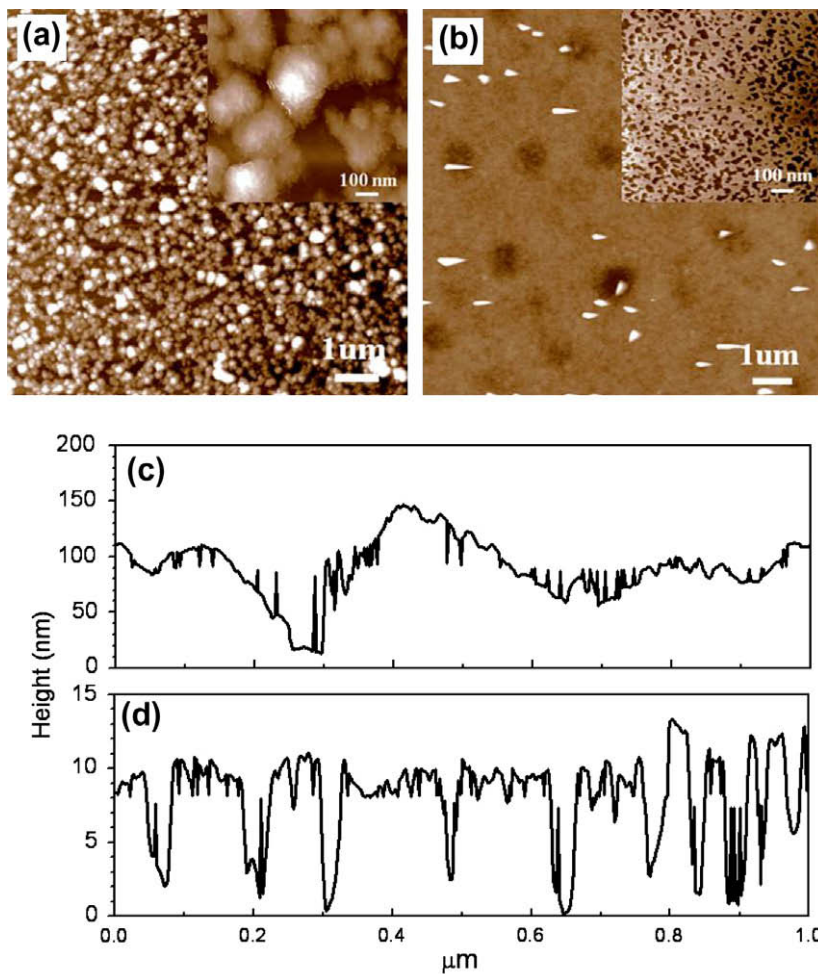
Fig. 4. (a) AFM image and (c) height profile of the film from N-TiO$_2$ solution, and (b) AFM image and (d) height profile of the film from OL-TiO$_2$ solution.

OL-TiO$_2$ interlayer helps the separation of subcell and forms better interfacial contact between the OL-TiO$_2$ and PEDOT:PSS layer. This implies that the recombination efficiency at the N-TiO$_2$/PEDOT:PSS interlayer will be significantly lower than that at the OL-TiO$_2$/PEDOT:PSS interlayer, which leads to voltage drop across the interface, and results in a lower V_{OC} of the TC-N [7].

These properties, however, were obtained after several repeated measurements under the 1 sun illumination. Fig. 6 shows the change in the photovoltaic properties of
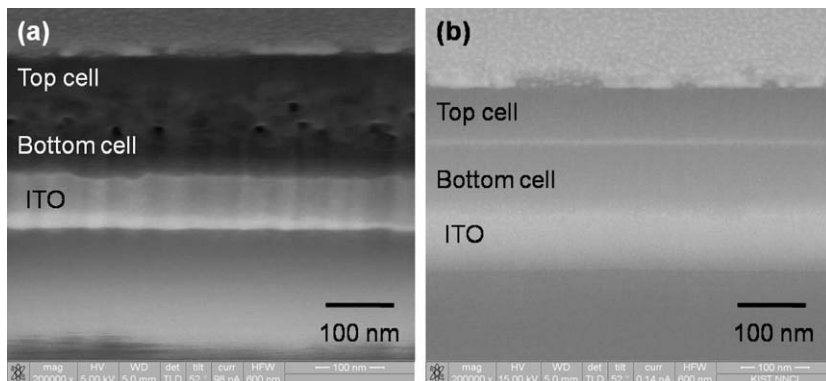

Fig. 5. The Focused Ion Beam (FIB) cross-sectional image of the polymer tandem cells (a) TC-N and (b) TC-OL.
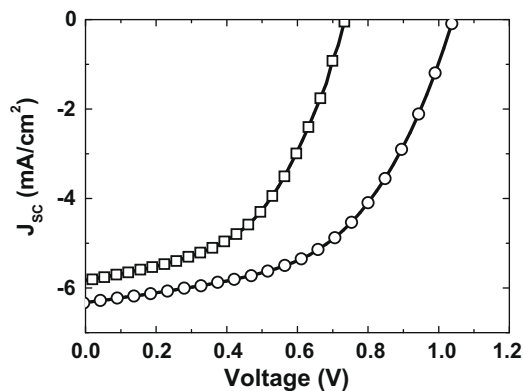
Fig. 6. Current density–voltage characteristics of a tandem cell utilizing OL-TiO$_2$ as interlayer before (square) and after (circle) AM 1.5G irradiation for 3 min.

Fig. 7. Influence of hole injection layer conductivity on the current density–voltage characteristics of single cells and tandem cells.

the TC-OL after 3 min of 1 sun illumination. As shown in Fig. 5, the J_{SC} and V_{OC} were increased from 5.83 mA/cm^2 to 6.33 mA/cm^2 and from 0.73 V to 1.04 V after the illumination, respectively. It is reported that the non-ohmic contact between metal oxide and the PEDOT layer could reduce the V_{OC} of the tandem cell [8]. The ohmic contact between the interface can be achieved by increasing the conductivity of the metal oxide and it can be improved by exposing the UV light on the metal oxide [12]. Since there is UV portion in the AM 1.5 light, it is possible that conductivity of the TiO$_2$ film can be increased by the AM 1.5 illumination.

Although the V_{OC} of the tandem cell was significantly increased by using OL-TiO$_2$, the V_{OC} is still lower than the sum of the V_{OC} of the bottom and top cells. In the polymer tandem solar cell having the TiO$_2$/PEDOT:PSS interlayer, electrons from the bottom cell recombine with the hole from the top cell, at the TiO$_2$/PEDOT:PSS interface. If the bottom cell generates more photo-current than the top cell, the excess electrons cannot recombine with the hole from the top cell, and will be accumulated at the interface between the bottom cell and the interlayer. The electron accumulation will partially compensate the built-in voltage across the bottom cell until the photo-current from the bottom cell matches with that of the top cell [7]. Moreover, excess electrons could act as a resister inside the bottom cell and reduce the fill factor of the cell. This results in a reduced performance of the tandem cell.

It was reported that photo-generated holes can be collected from the area where ITO electrode is not deposited due to the conductivity of the PEDOT:PSS [13]. Based on the report, it is highly possible that the mismatch of J_{SC} value between the bottom and top cells depends on the conductivity of PEDOT:PSS, which is used in the bottom cell, and this becomes significant as the conductivity of the PEDOT:PSS layer is increased. The photovoltaic properties of the single and tandem cells were examined by changing the conductivity of the PEDOT:PSS layer. The three different conductivities of the PEDOT:PSS solution, Baytron P VP AI 4083 (σ = 0.0002–0.002 S/cm), Baytron P (max σ = 0.1–1 S/cm), and Baytron PH 500 (σ = 10–50 S/cm), were used for the hole transporting layer (HTL) of the bot-
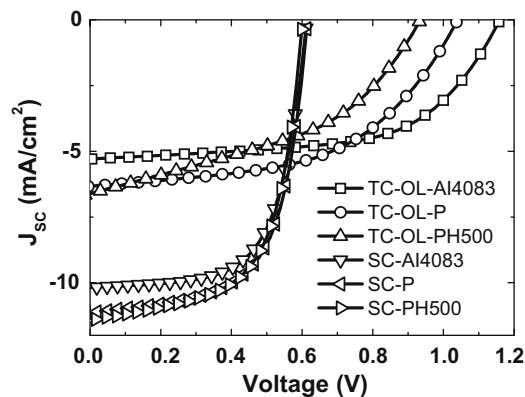
tom cell [14]. Hereafter, the tandem cell using Baytron P VP AI 4083, Baytron P and Baytron PH 500 as HTL for the bottom cell will be denoted as TC-OL-AI4083, TC-OL-P, and TC-OL-PH 500, respectively. As shown in Fig. 7 and Table 1, the J_{SC} of the single junction cell increased by increasing the conductivity of the PEDOT:PSS. This implies that the J_{SC} mismatch between the bottom and top cell of the tandem cell will be increased as the conductivity of PEDOT:PSS increases. The J_{SC} mismatch between subcells accommodates the charging of ITL and increase the internal resistance of the tandem cell, which resulted in the reduction of the V_{OC} and FF of the tandem cell. The J_{SC} of the tandem cell was decreased from 6.7 mA/cm^2 to 5.3 mA/cm^2 as the HTL of the bottom cell was changed from the highly conductive Baytron PH 500 (TC-OL-PH 500) to the less conductive Baytron P VP AI 4083 (TC-OL-AI4083). However the V_{OC} and FF of the TC-OL-AI4083 were significantly enhanced, in particular, the V_{OC} of the cell was almost doubled compared to that of the single junction cell. As a result, the power conversion efficiency of the TC-OL-AI4083 (3.66%) was 6%, and 37% higher than that of TC-OL-P and TC-OL-PH 500, respectively. Based on the experimental results, the conductivity of the PEDOT:PSS is considered to be closely related to $J_{SC,}$ V_{OC} and FF in the tandem cells.

However, the J_{SC} value of the tandem cell was significantly lower than that of the single cell. In order to optimize the photo-current of the tandem cell, we varied the thickness of the active layers of the top and the bottom cell. First, the thickness of active layer of the top cell (TL) was varied while maintaining the thickness of active layer of the bottom cell (BL) at 100 nm. Table 2 summarizes the photovoltaic performance of the tandem cell and Fig. 8(a) shows their I–V curves. The J_{SC} of the tandem cell was increased from 4.88 to 5.91 mA/cm^2 as the thickness of the TL increased from 70 to 200 nm. The highest photo-current of 5.91 mA/cm^2 was obtained from the T3 and the value is 21% higher than that from the T1. The external quantum efficiency (EQE) for these tandem cells (Fig. 9(a)) are consistent with the J_{SC} result of the tandem cells. The EQE of the tandem cell was increased at around 400 and 600 nm as the thickness of the top cell increased. Whereas, no

Table 1
The dependence of HIL conductivity on the performances of single cells and tandem cells having OL-TiO$_2$ interlayer.

HIL	ITL	V_{OC} (V)	J_{SC} (mA/cm^2)	FF	Efficiency (%)
Baytron P VP AI 4083		0.61	10.17	0.65	4.04
Baytron P		0.62	11.14	0.63	4.32
Baytron PH 500		0.60	11.42	0.62	4.26
Baytron P VP AI 4083	Baytron PH 500	1.16	5.3	0.60	3.66
Baytron P	Baytron PH 500	1.04	6.33	0.52	3.44
Baytron PH 500	Baytron PH 500	0.93	6.69	0.43	2.67

Table 2
The dependence of active layer thickness on the performances of single cells and tandem cells having OL-TiO$_2$ interlayer.

Cell type	Active layer thickness (nm)	V_{OC} (V)	J_{SC} (mA/cm^2)	FF	Efficiency (%)
Single junction					
S1	70	0.63	8.55	0.63	3.39
S2	100	0.62	10.25	0.63	4.04
S3	200	0.60	11.19	0.55	3.71
Tandem					
T1	100 (bottom)/70 (top)	1.05	4.88	0.52	2.62
T2	100 (bottom)/100 (top)	1.16	5.3	0.60	3.66
T3	100 (bottom)/200 (top)	1.07	5.91	0.48	2.97
T4	70 (bottom)/100 (top)	1.00	5.95	0.42	2.44
T5	200 (bottom)/100 (top)	1.02	3.16	0.59	1.89
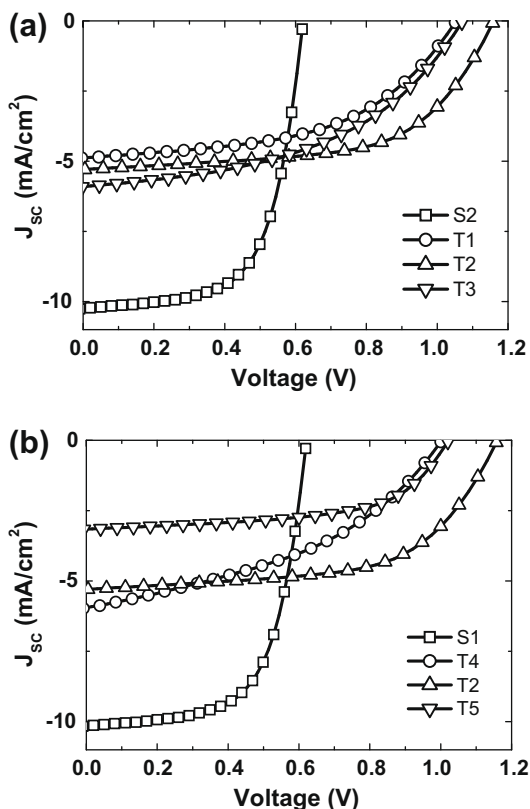
Fig. 8. The effects of varying the thickness of (a) top active layer (TL) and (b) bottom active layer (BL) on the current density–voltage characteristics of tandem cells. The detailed thicknesses of each active layer are listed in Table 2.
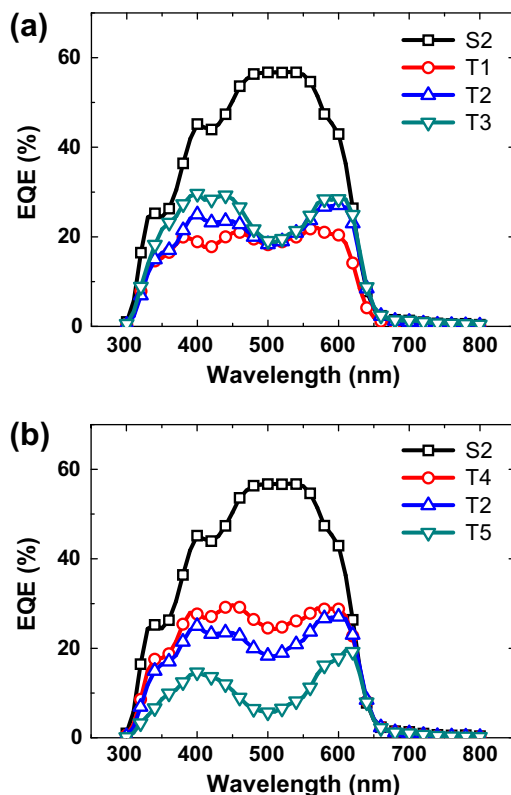
Fig. 9. External quantum efficiency (EQE) spectra of single cell and tandem cells with different active layer thickness of (a) the top cells and (b) bottom cells. The detailed thicknesses of each active layer are listed in Table 2.
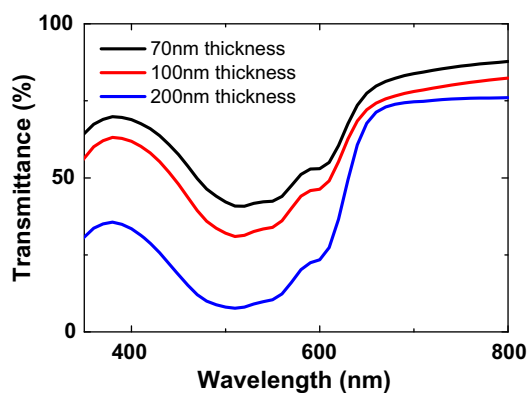
Fig. 10. Transmittance of P3HT:PCBM film with various thickness.

Fig. 11. Comparison of the cell stability under the 1 sun illumination for (a) a single cell (b) a tandem cell TC-OL. The stability test of the single and tandem cell were conducted without any passivation or glass encapsulation.

change in the EQE at 500 nm was observed by varying the thickness of the TL. This is related to the transmittance of the P3HT in the BL. The transmittance of 100-nm thick film of P3HT was about 30% at 500 nm (Fig. 10). This implies only 30% of incoming light of 500 nm wavelength can reach to the TL. Because P3HT has the largest molar extinction coefficient at the wavelength, thin layer of the TL (70 nm) is enough to absorb all the 500 nm light arriving on it. As a result, the EQE of the tandem cell at 500 nm is independent with the thickness of TL. On the other hand, the transmittance of the P3HT at around 400 and 600 nm is relatively higher than that at 500 nm due to the lower molar extinction coefficient. Because larger amount of 400 and 600 nm wavelength light reaches to the TL and P3HT in the TL has lower molar extinction coefficient at the wavelength, the EQE values of the tandem cell at the wavelengths are proportional to thickness of the TL.

For the next experiment, the thickness of the BL was varied while maintaining the thickness of active layer of the TL at 100 nm. The result of their photovoltaic performance and I–V curves are shown in Table 2 and Fig. 8(b). The J_{SC} of the tandem cell was increased from 3.16 to 5.95 mA/cm^2 as the thickness of BL decreased from 200 to 70 nm. The highest photo-current of 5.95 mA/cm^2 was obtained from the T4 and the value is 88% higher than that from the T5. The EQE of the tandem cell was inversely correlated with the thickness of BL without concerning the wavelength. Because the light arriving on the TL will be increased as decrease the thickness of BL. As a result of varying the thickness of active layer, the thinner BL (T4) or the thicker TL (T3) generated more photo-current than other tandem cells. Based on the experiments, it seems that the photo-current of our tandem cells are mainly determined by the photo-current generation from the top cell. However, the highest conversion efficiency was obtained from the tandem cell of T2 which has intermediate thickness (100 nm for the top and bottom cell). It is ascribed to the enhanced V_{OC} and FF of the T2 compare to the other tandem cells.

Interestingly, the tandem cell showed enhanced stability compared to the single cell (Fig. 11). The active layers of the cells were covered with commercial epoxy resin (Clear Epoxy, Dong Sung Uni. Tech. Co., Korea) in air before the
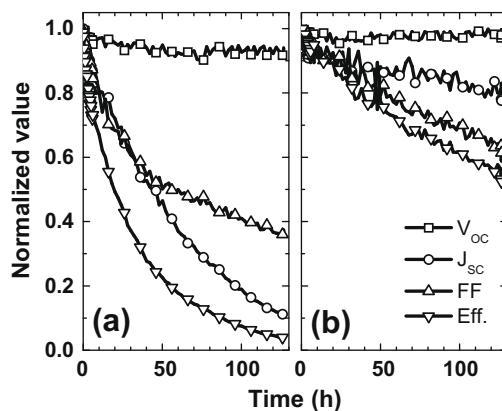
light soaking test. The stability of the cells was monitored by continuous irradiation under a sulfur plasma lamp. The light intensity of the lamp was adjusted using a NREL-calibrated mono Si solar cell with a KG-2 filter, for approximately AM 1.5G 1 sun light intensity. The temperature of the testing chamber was approximately 35 °C. Fig. 10 compares the stability of the TC-4083 and the single junction cell, and it was found that there was 94% degradation after 125 h irradiation for the single junction cell, whereas the TC-OL-4083 maintained 56% of its initial efficiency. The degradation is mainly ascribed to the decreased J_{SC} and FF for both the single and tandem cells. The decline of the J_{SC} and FF of the single cell was much faster than that of the tandem cell. It is thought that the better stability of the tandem cell is ascribed to the dense TiO$_2$ nanoparticles interlayer, which can protect the active layer in the bottom cell from the oxygen. Similar results have been reported, where the stability of a cell was enhanced by utilizing the TiO$_x$ as an electron transporting layer [15].

4. Conclusions

In conclusion, solution processed polymer tandem cells have been fabricated by utilizing the highly dispersive organic layer coated crystalline TiO$_2$ nanoparticles (OL-TiO$_2$)/ PEDOT:PSS interlayer. The top and bottom cell were clearly separated by the interlayer without interlayer mixing, which was not observed for the tandem cell utilizing commercially available TiO$_2$ nanoparticle (N-TiO$_2$) for the interlayer. The conversion efficiency of the polymer tandem cell was enhanced from 1.43% to 3.44% by replacing the interlayer from N-TiO$_2$ to OL-TiO$_2$. The J_{SC} of the tandem cell was increased by decreasing the bottom layer thickness or increasing the top layer thickness. This implies that the photo-current of our tandem cells are mainly determined by the photo-current generation from the top cell. However, the highest conversion efficiency was obtained from the tandem cell having intermediate thickness (100 nm for the top and bottom cell) due to the enhanced V_{OC} and FF by minimizing the charging of the excess charge

carriers at the interlayer. Based on the V_{OC}, J_{SC} and FF of the tandem cell, it is thought that the OL-TiO$_2$ layer performs the role of interlayer in the tandem cell with little loss of J_{SC} and V_{OC}. In addition that, it was found that the OL-TiO$_2$ interlayer enhanced the stability of the tandem cell comparing to that of the single junction cell. It could be ascribed to the reduction of the oxygen diffusion to the bottom layer by the interlayer. We believe the highly dispersive OL-TiO$_2$ has several advantages for the solution processed polymer solar cell in terms of excellent film forming property, crystallinity, transparency, stability and processability. It is expected that the performance of the tandem cell can be further enhanced by adopting efficient low band gap materials to the bottom cell.

Acknowledgements

Reference

[1] P. Wurfel, Physic of Solar Cells, Wiley-VCH, Weinhein, Germany, 2004.
[2] M. Hiramoto, M. Suezaki, M. Yokoyama, Chem. Lett. (1990) 327.
[3] A. Yakimov, S.R. Forrest, Appl. Phys. Lett. 76 (2000) 2650.
[4] G. Dennler, H.-J. Prall, R. Koeppe, M. Egginger, R. Autengruber, N.S. Sariciftci, Appl. Phys. Lett. 89 (2006) 073502.
[5] V. Shrotriya, E.H. Wu, G. Li, Y. Yao, Y. Yang, Appl. Phys. Lett. 88 (2006) 064104.
[6] K. Kawano, N. Ito, T. Nishimori, J. Skai, Appl. Phys. Lett. 88 (2006) 073514.
[7] A. Hadipour, B. de Boer, J. Wildeman, F.B. Kooistra, J.C. Hummenlen, M.G.R. Turbiez, M.M. Wienk, R.A.J. Janssen, P.W.M. Blom, Adv. Funct. Mater. 16 (2006) 1897.
[8] J. Gilot, M.M. Wienk, R.A.J. Janssen, Appl. Phys. Lett. 90 (2007) 143512.
[9] J.Y. Kim, K. Lee, N.E. Coates, D. Moses, T.-Q. Nguyen, M. Dante, A.J. Heeger, Science 317 (2007) 222.
[10] E. Kwak, W. Lee, N.-G. Park, J. Kim, H. Lee, Adv. Funct. Mat. 19 (2009) 1093.
[11] E. Scolan, C. Sanchez, Chem. Mater. 10 (1998) 3217.
[12] F. Verbakel, S.C.J. Meskers, R.A.J. Janssen, Appl. Phys. Lett. 89 (2006) 102103.
[13] M.-S. Kim, M.-G. Kang, L.J. Guo, J. Kim, Appl. Phys. Lett. 92 (2008) 133301.
[14] Product information of PEDOT:PSS (Baytron P VP AI 4083, P, PH 500) on CLEVIOS homepage. <http://www.clevios.com>, 2009.
[15] K. Lee, J.Y. Kim, S.H. Park, S.H. Kim, S. Cho, A.J. Heeger, Adv. Mater. 19 (2007) 2445.